Magnetic structure of $Co_{1-x}Mn_x$ alloys

D. Wu, G. L. Liu, C. Jing, Y. Z. Wu, D. Loison, G. S. Dong, and X. F. Jin*
Surface Physics Laboratory, Fudan University, Shanghai 200433, China

Ding-Sheng Wang
Institute of Physics, Chinese Academy of Sciences, Beijing 100080, China

(Received 23 October 2000; revised manuscript received 18 December 2000; published 30 April 2001)

$Co_{1-x}Mn_x$ thin films epitaxially grown on GaAs(001) have been studied using reflection high-energy electron diffraction, x-ray diffraction, and the magneto-optical Kerr effect. The result shows that Co-rich films are body-centered cubic and ferromagnetic, and Mn-rich ones are face-centered cubic and antiferromagnetic. However, the film structure and magnetism at $x \sim 0.5$ show strongly thickness-dependent behavior. The magnetic phases of ordered $Co_{1-x}Mn_x$ alloys ($x=0,1/4,1/2,3/4,1$) in both bcc and fcc structures have also been investigated by a first-principles linearized augmented plane-wave calculation in the local-spin-density approximation. With the help of the calculated results, the correlation established in experiment between the structure and magnetism of $Co_{1-x}Mn_x$ alloys is better understood.

DOI: 10.1103/PhysRevB.63.214403 PACS number(s): 75.50.Cc

I. INTRODUCTION

The correlation between the structure and magnetism of $3d$ transition-metal alloys has long been an important topic in condensed matter physics. Different chemical compositions in an alloy might lead to various crystallographic structures, which in turn can modify its magnetism. The efforts to investigate such a correlation are helpful in principle to reach a better understanding about itinerant magnetism, or even to manipulate these materials for specific desired magnetic properties. Among the $3d$ transition-metal alloys, the Mn-based alloys have recently attracted special attention because of their potential applications in the magnetic recording industry.[1–5] The $Co_{1-x}Mn_x$ alloy is one of them, and has shown interesting magnetic properties.[6–10] The magnetic phase diagram in bulk $Co_{1-x}Mn_x$ was established by Menshikov *et al.*,[7] and shows that $Co_{1-x}Mn_x$ is ferromagnetic with a hexagonal-close-packed structure for $0<x\leqslant 0.32$, but is antiferromagnetic with a face-centered-cubic structure for $0.32<x\leqslant 0.52$. For $x>0.52$, it is no longer possible to stabilize the fcc state.

However, it is known that epitaxial growth of materials on some appropriate substrate can drive the film into a specific crystalline structure. These structures may be in a thermodynamically stable bulk phase, a known high-pressure or high-temperature phase, or even a phase not previously observed. They greatly increase the variety of magnetic materials by essentially making ''new'' materials from ''old'' elements.[11] Body-centered-cubic Co, which does not exist in bulk phase, and face-centered-cubic Mn, which exists only at high temperature, were obtained by epitaxial growth on GaAs.[12–17] Motivated by these two results, we are curious to see what will happen if Co and Mn are codeposited to form $Co_{1-x}Mn_x$ alloys on a GaAs substrate, and what the correlation will be between its structure and magnetism as a function of composition.

In this work, the whole range of compositions ($0\leqslant x \leqslant 1$) has been experimentally explored for the growth of $Co_{1-x}Mn_x$ alloys on GaAs(001). The results show a fcc $Co_{1-x}Mn_x$ phase for $0.78<x\leqslant 1$, where no thermodynamically stable phases exists in the bulk material. A bcc $Co_{1-x}Mn_x$ phase, which does not exist in the bulk material, was also realized for $0\leqslant x<0.44$—a much broader range than we previously thought.[18] For $0.44\leqslant x\leqslant 0.78$, the $Co_{1-x}Mn_x$ films are bcc in the initial stage of growth; then a fcc phase starts to develop on top of the bcc phase as the film becomes thicker. Obviously the phase diagram obtained here for epitaxial $Co_{1-x}Mn_x$ films is very different from that of the bulk material; it is therefore interesting to study it and to establish the correlation between structure and magnetism. The magnetic measurements show that a $Co_{1-x}Mn_x$ film is ferromagnetic whenever its structure is bcc. On the other hand, it is antiferromagnetic whenever its structure is fcc. This strong correlation realized in experiment between the structure and magnetism of $Co_{1-x}Mn_x$ alloys was further studied and confirmed by a first-principles linearized augmented plane-wave (LAPW) calculation with the local-spin-density approximation (LSDA).

This paper is organized as follows. In Sec. II we describe first the growth and structure characterization by *in situ* reflection high-energy electron diffraction (RHEED) and *ex situ* x-ray diffraction, and then the magnetic measurement by the magneto-optical Kerr effect (MOKE). The first-principles calculation and its results for both bcc and fcc ordered $Co_{1-x}Mn_x$ alloys are presented and discussed in Sec. III. A summary is given in Sec. IV.

II. EXPERIMENT

$Co_{1-x}Mn_x$ films were grown in a molecular-beam epitaxy (MBE) growth chamber connected with a VG-ESCALAB-5 electron spectrometer system. Te-doped GaAs(001) single-crystal wafers were polished and treated by a standard cleaning process. The final substrate cleaning was performed using two different procedures. One is our routinely used method, i.e., argon ion bombardment followed by annealing. The other is a chemical etching method, using $H_2SO_4:H_2O_2:H_2O=5:1:1$, before loading into the MBE sys-

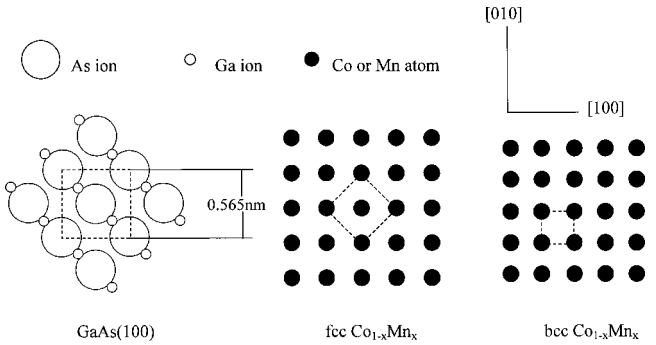

FIG. 1. Schematic top view of unreconstructed GaAs(001), together with rotated fcc $Co_{1-x}Mn_x(001)$ and unrotated bcc $Co_{1-x}Mn_x(001)$ surfaces.

tem and flashing to 580 °C in an ultrahigh vacuum chamber. We found in our experiment that the latter procedure provides better substrates for epitaxial films. The reconstruction pattern of (4×1) with streaks [caused by a random combination of (4×2) and $c(8\times2)$ (Ref. 19)] was observed by low-energy electron diffraction. Auger spectra show that the surfaces are free of carbon and oxygen contamination. 99.99% pure Mn and Co were charged into two separate Al_2O_3 crucibles of Knusden cells. The $Co_{1-x}Mn_x$ films were prepared by coevaporating Co and Mn on the GaAs(001) substrate at 400 K. The film thickness and composition of the $Co_{1-x}Mn_x$ alloys were calibrated and properly adjusted using a quartz thickness monitor, and further confirmed by Auger electron spectroscopy.

A. Growth and structure

GaAs(001) with the zinc-blende structure together with the corresponding Miller indices is illustrated in Fig. 1. In general, two kinds of epitaxial-growth geometry are expected for $3d$ transition metals and alloys on this substrate, i.e., the fcc structure with $(001)[110]_{\text{film}}\|(001)[100]_{\text{GaAs}}$ and the bcc structure with $(001)[100]_{\text{film}}\|(001)[100]_{\text{GaAs}}$. The lattice misfits between fcc-Co/GaAs and bcc-Co/GaAs are -10.8% and 0.1%, respectively, while the misfits between fcc-Mn/GaAs and bcc-Mn/GaAs are -8.6% and 2.3%, respectively. If the lattice match is the only concern, then a naive guess for the epitaxial structures of Co and Mn on GaAs(001) would be both bcc, because the bcc phases have much smaller misfits with the GaAs substrate than the fcc phases do. However, the experimental truth is that Co/GaAs(001) does have the bcc structure but Mn/GaAs(001) has the fcc structure. The mechanism of the unexpected behavior of Mn/GaAs(001) has been investigated and discussed in more detail elsewhere.[17] It was found that the interface structure played a key role in the formation of the fcc phase.

Spotlike RHEED diffraction patterns or a three-dimensional (3D) growth mode are normally observed in experiment for the growth of $3d$ transition metals and alloys on semiconductor substrates; a fingerprint recipe has been developed to distinguish between fcc and bcc structures.[16] We will use this simple procedure in the following to determine the $Co_{1-x}Mn_x$ film structure on the GaAs(001) substrate, since the spotlike diffraction patterns (or 3D growth mode) are indeed realized here.

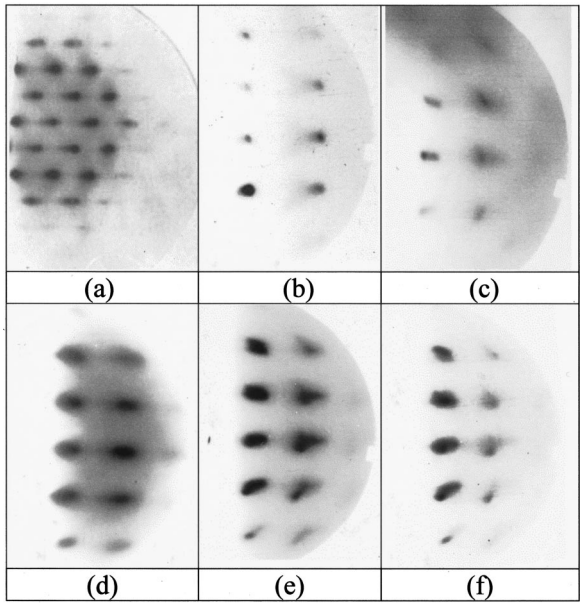

FIG. 2. Representative RHEED patterns of $Co_{1-x}Mn_x$/GaAs(001) in different Mn composition ranges. (a) Clean GaAs(001) surface; (b) bcc phase of $Co_{60}Mn_{40}$ films; (c) fcc phase of $Co_{10}Mn_{90}$ films; (d)–(f) thickness-dependent transition from bcc to fcc phase for $Co_{30}Mn_{70}$ film.

Figure 2 shows some representative RHEED patterns, with the incident electron beam along the $[1\bar{1}0]$ direction, for epitaxially grown $Co_{1-x}Mn_x$ films with different compositions. Figure 2(a) shows the RHEED pattern for a clean GaAs(001) surface, which serves as an internal scale to measure the film lattice constants. A typical RHEED pattern for the $Co_{1-x}Mn_x$ films with composition $0\leqslant x<0.44$ is shown in Fig. 2(b). The spotlike patterns represent transmission through 3D crystallites, which indicates island growth mode of the films. By using the recipe mentioned earlier,[16] it is easy to recognize that such a rectangular-shaped pattern must correspond to a bcc structure. Therefore it is known that the epitaxial Co-rich $Co_{1-x}Mn_x$ films are in a bcc phase, similar to that of Co on GaAs(001). Comparing to the preliminary result we obtained earlier,[18] it is noted here that this epitaxial bcc structure, which does not exist in bulk phase, actually covers a much wider range of composition than we previously thought. The in-plane lattice constants of the $Co_{1-x}Mn_x$ films at $x=0.4$, as shown in Fig. 2(b), are estimated to be $a=b=0.29$ nm, according to the RHEED pattern. However, it is difficult to determine the interlayer distance accurately from the RHEED patterns alone; thus x-ray diffraction measurements were carried out. For example, the interlayer lattice constant of $Co_{1-x}Mn_x$ at $x=0.4$ was determined to be 0.289 nm.

A typical RHEED pattern for $Co_{1-x}Mn_x$ with composition $0.78\leqslant x<1$ is shown in Fig. 2(c). By again using the recipe mentioned earlier, it is easy to recognize that such a square pattern must correspond to a fcc structure. Although

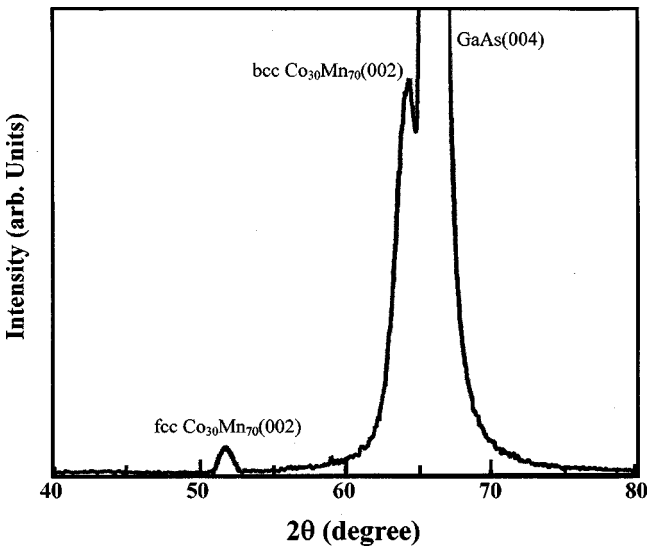

FIG. 3. X-ray diffraction spectra for 37 nm $Co_{30}Mn_{70}$ grown at 400 K.

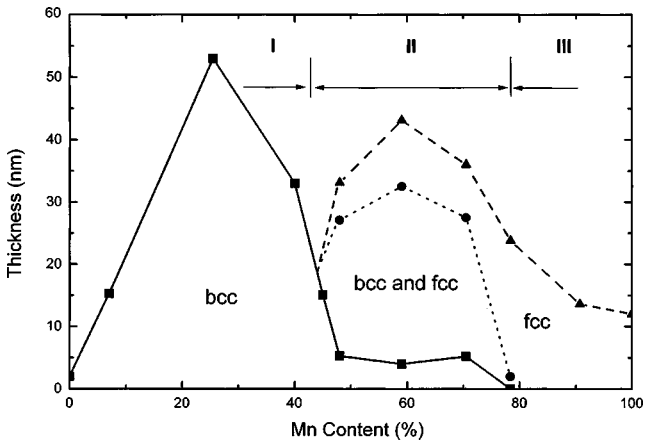

FIG. 4. Structural phase diagram for $Co_{1-x}Mn_x$ alloy films grown on GaAs(001).

no stable bulk phases of $Co_{1-x}Mn_x$ alloy can be obtained for $x>0.52$, the result here demonstrates that the epitaxial Mn-rich $Co_{1-x}Mn_x$ films are in a fcc phase, similar to that of Mn on GaAs(001). The in-plane lattice constants of the $Co_{1-x}Mn_x$ films at $x=0.9$, as shown in Fig. 2(c), are estimated to be $a=b=0.36$ nm according to the RHEED pattern. The interlayer lattice constant was determined to be 0.360 nm using x-ray diffraction.

However, the structure of the $Co_{1-x}Mn_x$ films in the range $0.44\leqslant x\leqslant 0.78$ is more complicated and shows thickness dependence. A typical case is given in Figs. 2(d)–2(f), where the RHEED patterns of a $Co_{30}Mn_{70}$ thin film were recorded at different growth stages to show the thickness dependence. In the initial stage at film thickness thinner than 5 nm, the film is bcc as shown by Fig. 2(d). As the film gets thicker, a mixture of rectangular- and squarelike diffraction patterns is observed, as shown in Fig. 2(e), indicating the coexistence of some fcc and bcc phases on top of the initial bcc film. In the final stage of growth for $\theta>27$ nm, the top-layer film has a fcc structure as shown in Fig. 2(f). The coexistence of fcc and bcc phases in the $Co_{1-x}Mn_x$ films with $x=0.70$ was further confirmed by x-ray diffraction measurement, as shown in Fig. 3. Both fcc and bcc peaks are clearly seen in this figure, from which the lattice constants for fcc and bcc phases are obtained as 0.361 and 0.295 nm, respectively. The thickness-dependent behavior of the $Co_{1-x}Mn_x$ films in the intermediate range of composition might be regarded as a result of competition between the tendencies to form fcc and bcc structures, since the growth of pure Co on GaAs(001) is in the bcc phase whereas pure Mn on GaAs(001) is in the fcc phase. Since in the intermediate composition range the bcc phase of the $Co_{1-x}Mn_x$ alloys has much smaller lattice misfit with the substrate ($\sim$1%) than the fcc phase ($\sim$9%), it is reasonable that the initial growth of $Co_{1-x}Mn_x$ on GaAs(001) is in the bcc phase. However, since the bcc phase of $Co_{1-x}Mn_x$ is a phase that does not exist in the bulk phase diagram, it is possible that $Co_{1-x}Mn_x$ tends to form the fcc phase when the film gets thicker. It is this competition that finally leads to the double-layer structure of the film with the fcc on top of the bcc phase, and the coexistence of the bcc and fcc patterns in Fig. 2(e) is just an indication of such a structural transition region. It is very unlikely that this bcc and fcc coexistence region corresponds to a phase separation into Mn-rich fcc and Co-rich bcc phases, otherwise the film structure in the final stage of growth would become much more complicated than the one we observed here in Fig. 2(f).

Based on the foregoing characterizations of the $Co_{1-x}Mn_x$ film structure in the whole range of compositions $0\leqslant x\leqslant 1$, we show in Fig. 4 a structural phase diagram as a function of composition. Three regions are clearly seen in this figure, i.e., the Co-rich bcc phase region marked I, the Mn-rich fcc phase region marked III, and the intermediate region with mixed bcc and fcc structures marked II. Since Co tends to grow in the bcc phase while Mn prefers to form the fcc phase on a GaAs(001) substrate, we believe that the different epitaxial structures of $Co_{1-x}Mn_x$ films are the results of competition. However, the detailed growth mechanism must depend not only on the strain due to the lattice mismatch between Co and Mn and GaAs(001), but also on the interface chemistry.[17]

With this structural phase diagram in mind, we carried out magnetic measurements in order to establish the correlation between structure and magnetism. Both polar and longitudinal magnetic hysteresis loops were measured for the $Co_{1-x}Mn_x$ films as a function of composition x, using the magneto-optical Kerr effect technique. Since the results show that they all have in-plane rather than out-of-plane magnetic easy axes, the discussion in the following will be focused only on the in-plane magnetism.

B. Magnetism

Some typical MOKE loops with different compositions, after being normalized for film thickness, are shown in Fig. 5. There are several facts to be noted in this figure. First, all the Co-rich $Co_{1-x}Mn_x$ films for $x<0.44$ exhibit strong ferromagnetism. Second, all the Mn-rich $Co_{1-x}Mn_x$ films for

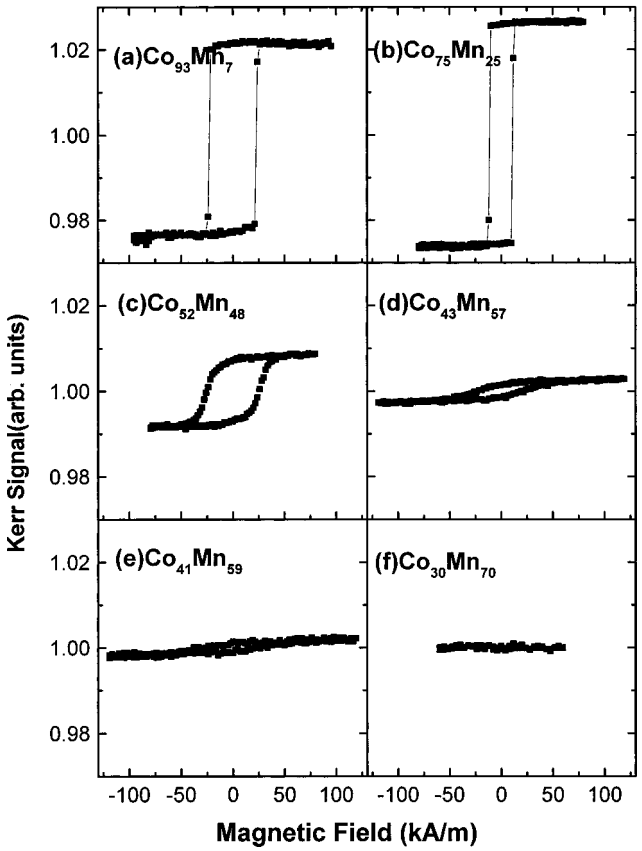

FIG. 5. Longitudinal MOKE hysteresis curves for $Co_{1-x}Mn_x$ alloys at different Mn compositions.

$x>0.78$ exhibit zero total magnetic moment, although it is unknown whether they are paramagnetic or antiferromagnetic. Last, the films with intermediate compositions $0.44 \leqslant x \leqslant 0.78$ show relatively weak ferromagnetism. It becomes clear from these results that a strong correlation does exist between the structure and magnetism for $Co_{1-x}Mn_x$ films, i.e., the bcc phase corresponds to ferromagnetism while the fcc phase corresponds to the absence of ferromagnetism.

However, it is still unclear why the magnetism becomes relatively weak in the intermediate composition region. Two options might exist: either the magnetic moment per atom is smaller for the whole film than for the Co-rich phase, or only part of the film is ferromagnetic and the rest of it does not contribute to the total magnetic moment. In order to distinguish these two different mechanisms, wedge-shaped samples were prepared and measured by the MOKE technique at room temperature. Figure 6 shows a typical curve from these measurements, where the Kerr intensity versus thickness for a $Co_{52}Mn_{48}$ film is given. A trilayer magnetic structure is realized in this figure, i.e., a magnetic dead layer ($\sim$2 nm) near the interface, a ferromagnetic layer in the middle, and a nonferromagnetic layer on the top. The explanation for this result is straightforward. The magnetic dead layer is presumably caused by the interface reaction between film and substrate, as is quite common in such systems. The linearly increasing Kerr intensity comes only from the bcc-dominated $Co_{52}Mn_{48}$ film. The saturated Kerr intensity is caused by the fact that the top layer has the fcc-dominated

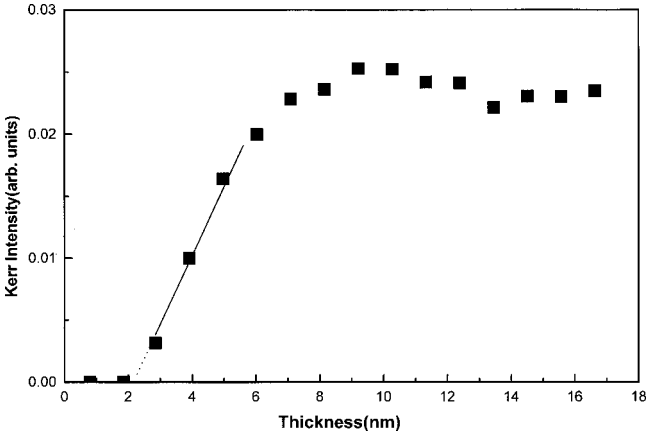

FIG. 6. Kerr intensity for wedge-shaped $Co_{52}Mn_{48}$ film at different thicknesses.

structure. Therefore, it is concluded from the above magnetic measurements that $Co_{1-x}Mn_x$ films are ferromagnetic if the structures are bcc, whereas they are not ferromagnetic if the structures are fcc. Furthermore, our preliminary results obtained from fcc-$Co_{1-x}Mn_x$/Fe bilayer systems indicate the existence of unidirectional exchange bias between fcc $Co_{1-x}Mn_x$ and Fe, leading to the conclusion that the fcc $Co_{1-x}Mn_x$ films are antiferromagnetic.

III. THEORETICAL CALCULATION

A correlation was established in experiment between the magnetism and structure of $Co_{1-x}Mn_x$ films, but its explanation is not trivial. For this purpose an *ab initio* all-electron linearized augmented plane-wave calculation in the local-spin-density approximation was carried out.[20] The main task here is to check whether the foregoing experimental results can be understood in principle based on the currently existing theoretical framework for itinerant magnetism.

Since $Co_{1-x}Mn_x$ alloys with both bcc and fcc structures have been observed in experiments as shown previously, we are going to investigate them separately in the following calculation. The models used are limited to chemically ordered $Co_{1-x}Mn_x$ alloys with compositions of $x=0,1/4,1/2,3/4,1$, which means only four atoms in each unit cell are considered for both bcc and fcc cases, as illustrated in Figs. 7(a) and 7(b), respectively. Although it is difficult to verify whether or not the model does represent the experiment correctly, we

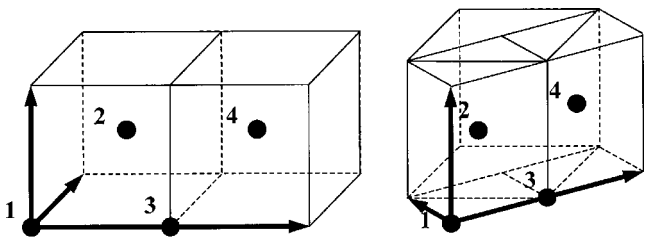

FIG. 7. Unit cells of $Co_{1-x}Mn_x$ alloys in calculation: (a) bcc and (b) fcc structure.

TABLE I. Lattice constants (nm) used in calculation for both bcc and fcc phases.

	x				
	0.00	0.25	0.50	0.75	1.00
fcc	0.354	0.357	0.360	0.362	0.365
bcc	0.283	0.285	0.286	0.288	0.289

think at least it serves as a reasonable working frame toward a better understanding of the real situation. The fact that $Co_{1-x}Mn_x$ films can grow epitaxially on the GaAs(001) surface excludes the possibility of macroscopically precipitated Co and Mn patches in the films, otherwise the lattice mismatch between them would prevent the films from being single crystalline. However, chemical disordering in the alloy films may very likely happen; this needs to be addressed in more detail with techniques such as extended x-ray absorption fine-structure (EXAFS) measurements, which is certainly beyond the scope of this paper. It should also be pointed out that neither magnetic configurations other than a collinear alignment nor magnetic structures with bigger unit cells are considered in this calculation.

The four atoms labeled 1, 2, 3, and 4 in Fig. 7 can be either Co or Mn atoms, representing $Co_{1-x}Mn_x$ alloys with different composition. Fifty plane waves per atom and 30 **k** points in the first irreducible Brillouin zone are used in the calculation. The self-consistency is better than 0.01 me/a.u.^{3} for charge density and spin density, and the stability is better than 0.1 mRy for the total energy per cell.

The lattice constants used in the calculation for pure Co and Mn are chosen in the following way. The lattice constants of 0.354 and 0.283 nm for fcc and bcc Co, respectively, are taken from experimental data.[12] The lattice constant of 0.365 nm for fcc Mn is also taken from the experimental value.[16] Since no experimental values for bcc Mn exist so far, a value of 0.289 nm is used based on the assumption that it has the same atomic density as α-Mn.[21] With these four numbers fixed, the lattice constants for both bcc and fcc $Co_{1-x}Mn_x$ alloys are then obtained by linear interpolation, as listed in Table I.

Based on the lattice constants given in Table I, the calculated total magnetic moments per unit cell as well as the individual atomic magnetic moments in each unit cell for both bcc and fcc $Co_{1-x}Mn_x$ alloys are obtained, as seen in Tables II and III, respectively. In the following we discuss the results for fcc and bcc phases separately.

A. fcc $Co_{1-x}Mn_x$ phase

As seen in Table II, the calculated result for the fcc $Co_{1-x}Mn_x$ alloy with $x=0$, i.e., pure fcc Co, shows that the four atomic spins in the unit cell are aligned parallel to each other to form ferromagnetic ordering, as expected. The magnetic moment for each spin is $1.7\mu_B$, which agrees quite well with that reported previously in the literature.[22–25]

For fcc $Co_{1-x}Mn_x$ alloy with $x=1$, i.e., pure fcc Mn, the calculated result gives antiferromagnetic ordering with the spins of atoms 1 and 3 antiparallel to those of atoms 2 and 4, which agrees with the result obtained previously by Fuster *et al.*, using a different method of calculation.[26] The magnetic moment for each spin is $2.1\mu_B$. Since no experimental data exist in the literature for pure fcc Mn, a direct comparison with our calculation is not available at this moment. However a value of $2.4\mu_B$ was obtained by extrapolation from the MnCu alloy, which is not too far from what we get here.[27]

TABLE II. Calculated atomic magnetic moments $(\mu_B)m(i)$ ($i=1,2,3,4$ as shown in Fig. 7) for bcc $Co_{1-x}Mn_x$ alloys. m_{av} means the average atomic moment per unit cell. The asterisk indicates Co atoms, and the rest are Mn atoms.

	x					
	0.00	0.25	0.05 I	0.50 II	0.75	1.00
$m(1)$	1.70*	1.07*	0.004*	1.06*	2.02	2.10
$m(2)$	1.70*	−2.14	−1.78	−2.18	−0.53*	−2.10
$m(3)$	1.70*	1.02*	0.004*	2.13	2.02	2.10
$m(4)$	1.70*	1.37*	1.79	1.18*	−2.30	−2.10
m_{av}	1.70	0.33	0.004	0.55	0.30	0.00

For the fcc $Co_{1-x}Mn_x$ alloy with $x=0.25$, the calculated result shows that the three Co spins are parallel to each other but are antiparallel to the Mn spin. The magnetic moments are $-2.14\mu_B$ for Mn, and $1.07\mu_B$, $1.02\mu_B$ and $1.37\mu_B$ for Co. This leads to an average net magnetic moment of $0.33\mu_B$ per atom in a unit cell. A direct comparison with experiment is not available, since the fcc $Co_{0.75}Mn_{0.25}$ alloy does not exist according to the phase diagram.[7]

For the fcc $Co_{1-x}Mn_x$ alloy with $x=0.5$, two different atomic configurations are possible in principle. If one of the Co atoms is put at position 1 in Fig. 7(b), then the type-I configuration means the arrangement with Co atoms at 1 and 3, and Mn atoms at 2 and 4. The calculated result for this case shows that the two Co spins are parallel to the Mn spin at 4 but antiparallel to the Mn spin at 2. The magnetic moments are $0.004\mu_B$ for both Co atoms, and $-1.78\mu_B$ and $1.79\mu_B$ for the Mn atoms. This leads to an average magnetic moment of $0.004\mu_B$ per atom in a unit cell, essentially antiferromagnetic ordering. On the other hand, the type-III configuration means the arrangement with Co atoms at 1 and 4,

TABLE III. Calculated atomic magnetic moments $(\mu_B)m(i)$ ($i=1,2,3,4$ as shown in Fig. 7) for fcc $Co_{1-x}Mn_x$ alloys. m_{av} means the average atomic moment per unit cell. The asterisk indicates Co atoms, and the rest are Mn atoms.

	x					
	0.00	0.25	0.50 I	0.50 II	0.75	1.00
$m(1)$	1.78*	1.73*	1.19*	1.71*	2.65	−0.50
$m(2)$	1.78*	3.02	2.77	1.93	1.58*	2.37
$m(3)$	1.78*	1.73*	1.19*	1.93	2.65	−0.50
$m(4)$	1.78*	1.87*	2.77	1.71*	−1.16	2.37
m_{av}	1.78	2.09	1.98	1.82	1.43	0.94

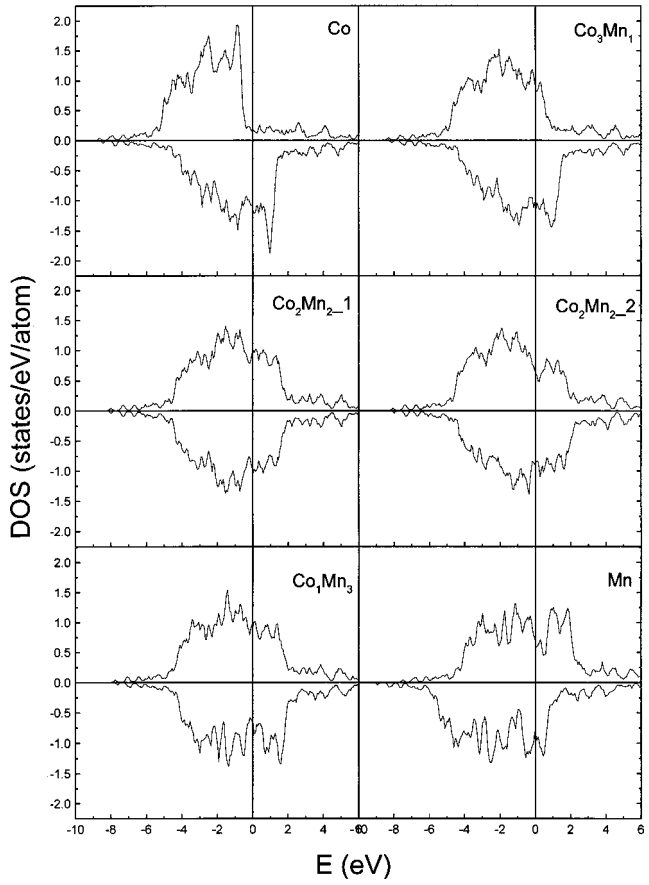

FIG. 8. Total density of states for majority and minority spins in the fcc phase.

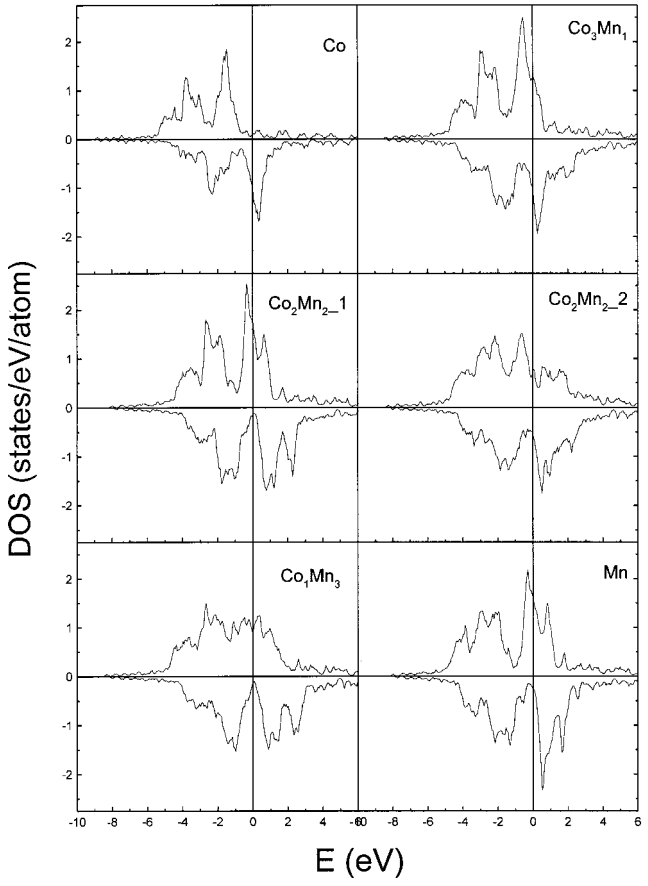

FIG. 9. Total density of states for majority and minority spins in the bcc phase.

and Mn atoms at 2 and 3. The calculated result for this case shows that the magnetic configuration is the same as type I, but the magnetic moments are very different, i.e., $1.06\mu_B$ and $1.18\mu_B$ for Co atoms and $-2.18\mu_B$ and $2.13\mu_B$ for Mn atoms. This leads to an average net magnetic moment of $0.55\mu_B$ per atom in a unit cell. Furthermore, according to our total-energy calculation, a small energy difference of 4 mRy per unit cell is found between types I and II, with the latter more favorable. However the experimental result of Menshikov *et al.*[7] revealed that the fcc $Co_{1-x}Mn_x$ alloy with $x=0.5$ is antiferromagnetic; meanwhile, our own experimental data also exclude the possibility of ferromagnetism. Therefore we tend to believe that the type-I configuration is actually closer to the real situation.

For the fcc $Co_{1-x}Mn_x$ alloy with $x=0.75$, the calculated result shows that the Co spin is parallel to the Mn 4 spin but antiparallel to the other two Mn spins. The magnetic moments are $-0.53\mu_B$ for the Co atom and $2.02\mu_B$, $2.02\mu_B$, and $-2.30\mu_B$ for the Mn atoms, leading to ferromagnetism with an average magnetic moment of $0.30\mu_B$ per atom in a unit cell. This result is in fact quite different from what we found in experiment, where we clearly showed that the system is antiferromagnetic. The discrepancy here could be because more complicated magnetic configurations other than collinear exist or because antiferromagnetism with longer periodicity should be taken into account.

We show in Fig. 8 for fcc $Co_{1-x}Mn_x$ alloys the calculated energy distribution curves of the density of states near the Fermi energy for both majority and minority spins.

B. bcc $Co_{1-x}Mn_x$ phase

As seen in Table III, the calculated result for the bcc $Co_{1-x}Mn_x$ alloy with $x=0$, i.e., pure bcc Co, shows that the four atomic spins in the unit cell are aligned parallel to each other to form ferromagnetic ordering as expected. The magnetic moment for each spin is $1.78\mu_B$. The experimental value of $1.4\mu_B$ was obtained by Prinz[12] in an epitaxial bcc Co film on a GaAs substrate. The agreement between these values is fairly good, taking into account that the measurement was done at room temperature instead of 0 K, and that the intermixing and chemical reaction at the interface might cause some magnetic dead layers.

For the bcc $Co_{1-x}Mn_x$ alloy with $x=1$, i.e., pure bcc Mn, the calculated result shows that the spins 1 and 3 are antiparallel to 2 and 4. The atomic magnetic moments are $-0.5\mu_B$ for spins 1 and 3, but $2.37\mu_B$ for spins 2 and 4, which leads to an average magnetic moment of $0.94\mu_B$ per atom in a unit cell. This result agrees with that obtained previously by Fuster *et al.*, using a different method of calculation.[26] Since no experimental data exist in the literature for pure bcc Mn, a direct comparison between our calculation and experiment is not available at this moment.

For the bcc $Co_{1-x}Mn_x$ alloy with $x=0.25$, the calculated result shows that all four spins are parallel to each other, resulting in ferromagnetic ordering. The magnetic moments are $1.73\mu_B$, $1.73\mu_B$, and $1.87\mu_B$ for the Co atoms and $3.02\mu_B$ for the Mn atom. This leads to an average magnetic moment of $2.09\mu_B$ per atom in a unit cell. Compared to the foregoing calculation for pure bcc Co, it is a little surprising that the total moment of the bcc $Co_{1-x}Mn_x$ alloy with $x=0.25$ is higher than that of the pure bcc Co. In fact this is exactly what was found in experiment as shown in Fig. 5.

For the bcc $Co_{1-x}Mn_x$ alloy with $x=0.5$, the calculated result shows that both types I and II are ferromagnetically ordered. The average magnetic moments per atom in a unit cell are $1.98\mu_B$ for type I and $1.82\mu_B$ for type II. On the other hand the total-energy calculation shows that the ground-state energy for type I is 125 mRy lower than that for type II. Therefore we tend to believe that what we have in the experiment is type I. Direct comparison with what we found in experiment, as shown in Fig. 5, seems to indicate a strong deviation from the calculation. However, taking into account the facts that the $Co_{0.5}Mn_{0.5}$ film grows in a mixed bcc and fcc phase, the fcc phase does not contribute the MOKE signal, and there are some dead layers in the bcc phase as well, the agreement between the calculation and experiment is not too bad.

For the bcc $Co_{1-x}Mn_x$ alloy with $x=0.75$, the calculated result shows that the Co spin and the Mn spins 1 and 3 are parallel to each other, but antiparallel to the Mn spin 4. The magnetic moments are $1.58\mu_B$ for Co, $2.65\mu_B$ for Mn 1 and 3, and $-1.16\mu_B$ for Mn 4, leading to an average magnetic moment $1.43\mu_B$ per atom in a unit cell. So far this remains only a theoretical prediction, because the bcc $Co_{1-x}Mn_x$ alloy with $x=0.75$ has not been obtained in experiment.

We show in Fig. 9 for bcc $Co_{1-x}Mn_x$ alloys the calculated energy distribution curves of the density of states near the Fermi energy for both majority and minority spins.

It should be pointed out that the foregoing calculated results are obtained only for bcc and fcc phases of $Co_{1-x}Mn_x$ alloys. However, the tetragonal distortion effect has also been considered and checked in the calculation. It turns out that the overall arguments obtained here from the cubic structures will not be changed for small distortions ($\sim$ a few percent), but the result will be significantly different for large distortions, as expected.

IV. CONCLUSION

In conclusion, it was shown in this work that the $Co_{1-x}Mn_x$ alloy grown on GaAs(001) has a bcc structure for $0\leqslant x<0.44$, a fcc structure for $0.78<x\leqslant 1$, and a double-layer structure with fcc on top of bcc for $0.44\leqslant x\leqslant 0.78$. The magnetism of the $Co_{1-x}Mn_x$ film is ferromagnetic for the bcc phase and antiferromagnetic for the fcc phase. This strong correlation between structure and magnetism has been further explored by an *ab initio* LAPW calculation, which indicates that the overall results obtained in the experiment can be explained in the theoretical framework of itinerant electron magnetism within the LSDA approximation.

ACKNOWLEDGMENTS

This work was supported by the National Natural Science Foundation of China, the Cheung Kong Program, the Hong Kong Qiushi Science Foundation, and the Y. D. Fok Education Foundation.

*Corresponding author. Email address: xfjin@fudan.ac.cn

[1] B. Dieny, V. S. Speriosu, B. A. Gurney, S. S. P. Parkin, D. R. Whilhoit, K. P. Roche, S. Metin, D. T. Peterson, and S. Nadimi, J. Magn. Magn. Mater. **93**, 101 (1991).

[2] T. Sands, J. P. Harbison, M. L. Leadbeater, S. Allen, Jr., G. W. Hull, R. Ramesh, and V. G. Keramidas, Appl. Phys. Lett. **57**, 2609 (1990).

[3] M. Tanaka, J. P. Harbison, J. Deboeck, T. Sands, B. Philips, T. L. Cheeks, and V. G. Keramidas, Appl. Phys. Lett. **62**, 1565 (1993).

[4] M. Tanaka, Mater. Sci. Eng., B **31**, 117 (1995).

[5] J. Deboeck *et al.*, Microelectron. J. **27**, 383 (1996).

[6] M. Matsui, T. Ido, K. Sato, and K. Adachi, J. Phys. Soc. Jpn. **28**, 791 (1970).

[7] A. Z. Menshikov, G. A. Takzei, Yu. A. Dorofeev, V. A. Kazanstev, A. K. Kostyshin, and I. I. Sych, Zh. Eksp. Teor. Fiz. **89**, 1269 (1985) [Sov. Phys. JETP **62**, 734 (1985)].

[8] M. Acet, C. John, and E. F. Wassermann, J. Appl. Phys. **70**, 6556 (1991).

[9] D. J. Rogers, Y. Maeda, and K. Takei, J. Appl. Phys. **78**, 5842 (1995).

[10] T. Thomson, P. C. Reidi, Q. Wang, and H. Zabel, J. Appl. Phys. **79**, 6300 (1996).

[11] L. M. Falicov, D. T. Pierce, S. D. Bader, R. Gronsky, K. B. Hathaway, H. Hopster, D. N. Lambeth, S. S. Parkin, G. A. Prinz, M. Salamon, I. K. Schuller, and R. H. Victora, J. Mater. Res. **5**, 1299 (1990).

[12] G. A. Prinz, Phys. Rev. Lett. **54**, 1051 (1985).

[13] S. J. Blundell, M. Gester, J. A. C. Bland, C. Daboo, E. Gu, M. J. Baird, and A. J. R. Ives, J. Appl. Phys. **73**, 5948 (1993).

[14] Y. Z. Wu, H. F. Ding, C. Jing, D. Wu, G. L. Liu, V. Gordon, G. S. Dong, and X. F. Jin, Phys. Rev. B **57**, 11 935 (1998).

[15] C. Jing, Y. Z. Wu, Z. X. Yang, G. S. Dong, and X. F. Jin, J. Magn. Magn. Mater. **198–199**, 269 (1999).

[16] X. F. Jin, M. Zhang, G. S. Dong, M. Xu, Y. Chen, Xun Wang, X. G. Zhu, and X. L. Shen, Appl. Phys. Lett. **65**, 3078 (1994).

[17] X. F. Jin, Yong Chen, X. W. Lin, G. S. Dong, Yan Chen, M. Xu, W. R. Zhu, Xun Wang, X. L. Shen, and L. Li, Appl. Phys. Lett. **70**, 2455 (1997).

[18] G. S. Dong, Y. Z. Wu, C. Jing, Y. Chen, W. R. Zhu, and X. F. Jin, J. Cryst. Growth **187**, 444 (1998).

[19] X. F. Jin, M. R. Yu, F. R. Zhu, and X. Wang, Semicond. Sci. Technol. **1**, 293 (1986).

[20] M. Dosternak, H. Krakauer, A. J. Freeman, and D. D. Koelling, Phys. Rev. B **21**, 5601 (1980); D. S. Wang, A. J. Freeman, H. Krakauer, and M. Dosternak, *ibid.* **23**, 1685 (1981); W. T. Geng, Y. M. Zhou, and D. S. Wang, Chin. J. Comput. Phys. **16**, 372 (1999).

[21] B. J. Jonker, J. J. Krebs, and G. A. Prinz, Phys. Rev. B **39**, 1399 (1989).
[22] C. Li, A. J. Freeman, and C. L. Fu, J. Magn. Magn. Mater. **75**, 53 (1988).
[23] H. P. Oepen, M. Benning, H. Ibach, C. M. Schneider, and J. Kirschner, J. Magn. Magn. Mater. **86**, L137 (1990).
[24] C. A. Chang, J. Magn. Magn. Mater. **109**, 243 (1992).
[25] R. Wu and A. J. Freeman, J. Magn. Magn. Mater. **116**, 202 (1992).
[26] G. Fuster, N. E. Brener, J. Callaway, J. L. Fry, Y. Z. Zhao, and D. A. Papaconstantopoulos, Phys. Rev. B **38**, 423 (1988).
[27] N. Cowlam and A. M. Shamah, J. Phys. F: Met. Phys. **11**, 27 (1981).